



Royal Netherlands Academy of Arts and Sciences (KNAW) KONINKLIJKE NEDERLANDSE AKADEMIE VAN WETENSCHAPPEN

Brain-wide induction of Δ FOSB and altered co-activation networks in a rat model for exercise training

Hardonk, Marene H; Vuuregge, Anna H; Hellings, Tom P; Eggels, Leslie; Ritsema, Wayne I G R; Lamuadni, Khalid; Unmehopa, Unga A; Meerhoff, Gideon F; Kalsbeek, Andries; Lucassen, Paul J; Schrantee, Anouk; la Fleur, Susanne E; Mul, Joram D

published in

Translational Psychiatry
2026

DOI (link to publisher)

[10.1038/s41398-026-03953-3](https://doi.org/10.1038/s41398-026-03953-3)

document version

Publisher's PDF, also known as Version of record

[Link to publication in KNAW Research Portal](#)

citation for published version (APA)

Hardonk, M. H., Vuuregge, A. H., Hellings, T. P., Eggels, L., Ritsema, W. I. G. R., Lamuadni, K., Unmehopa, U. A., Meerhoff, G. F., Kalsbeek, A., Lucassen, P. J., Schrantee, A., la Fleur, S. E., & Mul, J. D. (2026). Brain-wide induction of Δ FOSB and altered co-activation networks in a rat model for exercise training. *Translational Psychiatry*. Advance online publication. <https://doi.org/10.1038/s41398-026-03953-3>

General rights

Copyright and moral rights for the publications made accessible in the public portal are retained by the authors and/or other copyright owners and it is a condition of accessing publications that users recognise and abide by the legal requirements associated with these rights.

- Users may download and print one copy of any publication from the KNAW public portal for the purpose of private study or research.
- You may not further distribute the material or use it for any profit-making activity or commercial gain.
- You may freely distribute the URL identifying the publication in the KNAW public portal.

Take down policy

If you believe that this document breaches copyright please contact us providing details, and we will remove access to the work immediately and investigate your claim.

E-mail address:

pure@knaaw.nl

Brain-wide induction of Δ FOSB and altered co-activation networks in a rat model for exercise training

Received: 22 July 2025

Revised: 13 February 2026

Accepted: 6 March 2026

Cite this article as: Hardonk, M.H., Vuuregge, A.H., Hellings, T.P. *et al.* Brain-wide induction of Δ FOSB and altered co-activation networks in a rat model for exercise training. *Transl Psychiatry* (2026). <https://doi.org/10.1038/s41398-026-03953-3>

Marene H. Hardonk, Anna H. Vuuregge, Tom P. Hellings, Leslie Eggels, Wayne I.G.R. Ritsema, Khalid Lamuadni, Unga A. Unmehopa, Gideon F. Meerhoff, Andries Kalsbeek, Paul J. Lucassen, Anouk Schrantee, Susanne E. la Fleur & Joram D. Mul

We are providing an unedited version of this manuscript to give early access to its findings. Before final publication, the manuscript will undergo further editing. Please note there may be errors present which affect the content, and all legal disclaimers apply.

If this paper is publishing under a Transparent Peer Review model then Peer Review reports will publish with the final article.

Brain-wide induction of Δ FOSB and altered co-activation networks in a rat model for exercise training

Running title: Exercise and brain-wide chronic neuronal activation

Marene H. Hardonk¹, Anna H. Vuuregge^{1,2}, Tom P. Hellings¹, Leslie Eggels^{3,4,5}, Wayne I.G.R. Ritsema^{3,4,5}, Khalid Lamuadni^{3,4,5}, Unga A. Unmehopa^{3,4,5}, Gideon F. Meerhoff¹, Andries Kalsbeek^{3,4,5}, Paul J. Lucassen^{1,2}, Anouk Schranter^{2,6}, Susanne E. la Fleur^{2,3,4,5}, Joram D. Mul^{1,2,7#}

¹ Brain Plasticity group, Swammerdam Institute for Life Sciences, Amsterdam Neuroscience, Faculty of Science, University of Amsterdam, Amsterdam, the Netherlands

² Centre for Urban Mental Health, University of Amsterdam, Amsterdam, the Netherlands

³ Amsterdam UMC, University of Amsterdam, Laboratory of Endocrinology, Department of Laboratory Medicine, Amsterdam, the Netherlands

⁴ Amsterdam Gastroenterology, Endocrinology and Metabolism (AGEM), Amsterdam, the Netherlands

⁵ Netherlands Institute for Neuroscience, Institute of the Royal Netherlands Academy of Arts and Sciences (KNAW), Amsterdam, the Netherlands

⁶ Amsterdam UMC, University of Amsterdam, Department of Radiology and Nuclear Medicine, Amsterdam, the Netherlands

⁷ Amsterdam Neuroscience, Mood Anxiety Psychosis Stress and Sleep, Amsterdam, the Netherlands

Correspondence: Joram D. Mul (j.d.mul@uva.nl), Swammerdam Institute for Life Sciences, Faculty of Science, University of Amsterdam, Science Park 904, 1098 XH, Amsterdam, the Netherlands

Number of pages: 32

Number of figures: six main figures and nine supplementary figures

Number of tables: four supplementary tables

Abstract: 250 words

Introduction: 559 words

Materials & Methods: 1963 words

Results: 1814 words

Discussion: 1593 words

Full text: 5929 words (max. 5000 words)

ABSTRACT (250/250 words)

Exercise training promotes brain health, yet the underlying mechanisms remain unclear. Δ FOSB, a transcription factor involved in neuroplasticity, stress-, cognition- and reward-related behavior, accumulates in response to repetitive neuronal stimulation due to its unusual protein stability and can thus serve as a proxy for chronic neuronal activation. This study employed voluntary wheel running (VWR), an animal model for exercise training, in male and female Wistar rats to quantify VWR-induction of Δ FOSB in 44 brain regions implicated in stress, cognition and reward. Using network analysis, we examined broader patterns of co-activation and changes in network topology (*e.g.* centrality, small-world-likeness) of this comprehensive map of brain regions. Four weeks of VWR improved metabolic health, independent of sex, and females ran more than males. Notably, semi-automated quantification of Δ FOSB-immunoreactivity revealed VWR regulation of Δ FOSB in several cortical, striatal, hippocampal, hypothalamic and midbrain regions, which was more pronounced in females. VWR altered several parameters of Δ FOSB co-activation networks, decreasing network density while increasing global efficiency in both sexes, and was associated with greater cortical centrality. These findings demonstrate that VWR-mediated chronic neuronal activation extends beyond previously studied brain regions and that habitual VWR shifts hierarchy to more cortical regions. Because Δ FOSB overexpression is associated with lower neuronal excitability, the current Δ FOSB brain atlas and network co-activation dataset extends our understanding of the impact of VWR on brain neuroplasticity and provides a framework for future mechanistic studies into Δ FOSB-mediated changes in neuronal excitability during habitual VWR and subsequent effects on stress-, cognition- and reward-related behavior.

Introduction (559/1500 words)

Exercise training has numerous health benefits in the brain, including greater neuroplasticity, reduced risk for neurodegenerative and mental health-related disorders, and beneficial effects on cognition and substance abuse. Despite the clinical importance of these beneficial effects, the underlying brain mechanisms remain unclear. Understanding the neurobiological processes that mediate exercise training-induced improvements in stress-, cognition- and reward-related behavior, and whether these differ between sexes, can help optimize future therapeutic strategies based on physical activity to promote brain health in men and women, including beneficial effects on mental health, cognition, reward-related behavior, and healthy aging.

Mechanistic studies in rodents have identified the transcription factor Δ FOSB as a molecular mechanism driving neuroplasticity and long-term adaptation during diverse conditions, such as depression, antidepressant treatment, drug addiction, Parkinson's disease treatment, Alzheimer's Disease, adult hippocampal neurogenesis, epilepsy and learning and memory (1–17). Δ FOSB, part of the FOS family of immediate early genes, regulates gene expression via self-assemblies and heterodimerization with JUN proteins to form activator protein-1 transcription complexes (18–21). Due to structural modifications, Δ FOSB has a remarkable long half-life and can persist for days to weeks in neurons where it further accumulates upon repetitive stimulation (22–27). This makes Δ FOSB an attractive proxy to map chronic neuronal activation in a brain-wide manner. Functionally, mice that are resilient to chronic social stress are hallmarked by induction of Δ FOSB in specific subpopulations of nucleus accumbens (NAc) or ventral hippocampus (vHPC) neurons, which was associated with altered gene expression and neuronal plasticity in these neurons (13,15,28,29). Furthermore, viral-mediated overexpression of Δ FOSB in mouse dorsal HPC (dHPC) or vHPC decreased neuronal excitability (12,13). Thus, Δ FOSB mediates long-lasting molecular, structural, and functional adaptations in neuronal circuits involved in stress-, cognition- and reward-related behavior (2,20,28,30).

Long-term voluntary wheel running (VWR), a rodent model for exercise training, can be effectively used to identify molecular mechanisms underlying exercise-induced improvements in stress-, cognition- and reward-related behavior, including Δ FOSB-dependent processes (31–

33). For example, long-term (3-6 weeks) VWR increased Δ FOSB in several stress-related brain regions, including rat and mouse NAc (34–38) and mouse dHPC and vHPC (39), which can have functional implications for VWR-induced changes in stress-, cognition- and reward-related behavior. Indeed, we previously showed that long-term VWR increased resilience to chronic social stress, and that functional impairment of Δ FOSB in the NAc negated these protective effects (36). VWR also repressed Δ FOSB, as reported for the prairie vole basolateral amygdala (40) and rat suprachiasmatic nucleus (41), indicating a region-specific bilateral modulation of Δ FOSB, which suggests that regional differences in its expression may contribute to the VWR-mediated stress resilience.

While VWR is known to modulate Δ FOSB in specific brain regions, more complex behaviors, like mood, emerge from the coordinated activity of neuronal networks. Hence, a broader, brain-wide map of all Δ FOSB changes would not only provide a more complete overview of the patterns of chronic brain activation following long-term VWR, but would also allow to identify novel brain regions potentially involved in VWR-induced changes in stress-, cognition- and reward-related behavior, and explore the connectivity between such brain regions. To do this, we used an atlas-based semi-automated analysis approach (42) and assessed how four weeks of VWR in male and female Wistar rats, a duration sufficient to induce stable Δ FOSB accumulation and neural plasticity in limbic and cortical circuits (36,38–41), modulated Δ FOSB expression patterns in 44 brain regions linked to stress-, cognition- and reward-related behavior. We then used this Δ FOSB brain-wide map to investigate how VWR impacts Δ FOSB co-activation networks.

Materials and methods (1963 words)**Ethics approval**

All experimental procedures were performed in accordance with the European guidelines for laboratory animals (EU directive 2010\63\EU) and approved by the Dutch Central Committee for Animal Experiments (CCD; AVD8010020172424) and the Agency for Animal Welfare (IvD) of the Netherlands Institute of Neuroscience (NIN; Royal Dutch Academy of Sciences), Amsterdam.

Animals

We used 24 male (220-260g) and 24 female (170-210g) Wistar WU rats [8 weeks old; Crl:WI(WU), strain code 619, Charles River, Germany]. Males were studied in two separate cohorts (n = 12/cohort) and females in one cohort (n = 24/cohort). Rats were housed at the NIN animal facility in a temperature- (21-23°C), humidity- (40-60%) and light-controlled room [12:12h light/dark cycle, 280 (\pm 80) Lux, lights on; <5 Lux, lights off] with lights on at Zeitgeber time 0 (ZT0; 07:00). Continuous and soft radio functioned as background noise. To acclimate, rats were group-housed (4/cage) in a polycarbonate type 4 cage [53 x 33 x 20cm; 1749cm²; Plexx] for one week upon arrival. During acclimatization and the actual experiments, cages contained corncob bedding, enrichment (aspen wood gnawing stick, Technilab-BMI; PVC shelter, Bio Services) and rats had *ad libitum* access to a bottle of tap water (except for sucrose preference test, see below) and a high-carbohydrate pelleted diet (Teklad global diet 2918, 18.6% protein, 44.2% carbohydrate, and 6.2% fat, 3.1 kcal/g, Envigo).

Energy homeostasis and VWR

Following acclimatization, rats were individually housed in polycarbonate type 3H cages (37.5 x 21.5 x 18cm; 806cm²; Plexx) with standard diet and two bottles of water. All rats were housed in open cages within the same experimental room to allow sensory contact, helping to mitigate effects of individual housing, which was necessary to measure individual running distances and caloric intake. Baseline food and water intake were measured daily for four days. Then, to test if sucrose reward can predict subsequent running reward, a sucrose preference test (SPT) was performed by replacing one water bottle with 1% sucrose water, and food and liquid intake was

again measured daily for three days. Bottles were swapped daily to prevent a side bias. Following this seven-day baseline period, rats were randomized by body weight into two experimental groups: half remained housed sedentary (SED; male, $n = 12$; female $n = 12$), whereas the other half were housed in custom-made cages (42.2 x 42.22 x 47.5cm, 1781cm²) with free access to a vertical running (RUN) wheel (male = 12; female = 12; 34 cm diameter; 10 cm width; 1.068m/revolution) for 28 days. Sample sizes were determined based on prior experience with VWR experiments and previous experiments of comparable design. Wheel revolutions were continuously recorded using custom-made software (Cage Registration Program, Dep. Biomedical Engineering, UMC Utrecht, The Netherlands) (43). Body weight, food and water intake were measured weekly. To promote estrous cycle synchronization, two male transgenic ChAT::Cre Long-Evans rats were housed with the females and a vaginal smear was taken to determine estrous stage at the time of death. As the presence of the running wheel revealed group assignment, experimenters were not blinded to the experimental condition. However, all data collection and analyses were performed by investigators blinded to group identity.

Determination of estrous stage

Vaginal epithelial cells were collected using sterile plastic swabs (#861.562.010, Sarstedt BV), transferred onto glass slides (#631-0457, VWR), and air-dried overnight at room temperature. Smears were stained with Giemsa solution (#48900-100ML-F, Merck) for 10 min, rinsed three times with 1X tris-buffered saline (TBS; 50 mM Tris-Cl, 150 mM NaCl; pH 7.6), and subsequently dried overnight at room temperature (RT). Estrous stage was determined under a light microscope (DM2000, Leica) based on standard cytological criteria.

Tissue collection and single-labeling immunohistochemistry

To ensure degradation of full-length FOSB protein and isolate Δ FOSB accumulation during the VWR period, running wheels were blocked twenty-four hours prior to sacrifice (44,45). After 28 days of running and the 24h wheel blockade, rats were fasted for 1-6 hours before sacrifice between ZT0 and ZT6 via an overdose of sodium-pentobarbital. The left gonadal white adipose

tissue (gWAT) pad and both adrenals were quickly removed and weighed prior to transcardial perfusion with ice-cold 0.9% saline followed by ice-cold 4% paraformaldehyde (PFA) in 0.1M phosphate-buffered saline (PBS; pH 7.4). Removed brains were stored overnight in 4% PFA at 4°C, then washed and transferred to 30% sucrose in TBS with 0.05% sodium azide and stored at -80°C once saturated. Coronal brain sections (35µm) were cut on a cryostat (Leica CM1950) and stored in cryoprotectant medium (30%v/v glycerol, 30%v/v glycerinaldehyde and 40%v/v 0.1M PBS) at -20°C. Sections containing the cortex, basal ganglia/septum, hippocampus, (extended) amygdala, thalamus, hypothalamus and midbrain were collected from Bregma 5.16 till 0.36 and -1.08 till -6.72 (males) and Bregma 5.64 till 0.60 and -0.48 till -6.72 (females). For visualization of Δ FOSB, free-floating sections were washed in TBS and pre-treated with 10% methanol and 3% H₂O₂ (Merck) in TBS for 10 minutes to block endogenous peroxidase activity. Sections were then washed in TBS and incubated with rabbit anti-FOSB (5G4; #2251, Cell Signaling Technology, RRID: AB_2106903), diluted 1:3000 in supermix (0.25% w/v gelatin, 0.5% v/v Triton X-100, in 1x TBS, pH 7.6) for 1h at RT and overnight at 4 °C. After washing in TBS, sections were incubated with 1:400 biotinylated goat anti-rabbit IgG (H + L) (BA-1000; Vector Laboratories, Burlingame, RRID: AB_2313606) for 1h at RT. Following washing with TBS, Avidin-Biotin complex (Vectastain Elite ABC HRP Kit, PK-6100, Vector Laboratories) diluted 1:800 in supermix was added for amplification, followed by signal detection using DAB as a chromogen (0.05% w/v 3,3'-diaminobenzidine (Sigma), 0.23% w/v nickelammoniumsulphate (Merck) and 0.01% w/v H₂O₂ (Merck) in 0.05M TB, pH 7.6). The reaction was stopped in ultrapure H₂O and sections were washed in TBS. Hereafter, sections were mounted onto Superfrost Plus slides (Thermo Scientific) and air-dried O/N. Slides were dehydrated using increasing concentrations of ethanol, followed by xylene, and coverslipped with Entellan (#107961, Merck).

Image acquisition and analysis

For unbiased quantification, immuno-stained sections were randomly numbered and scanned using a Zeiss Axio Scan.Z1 slide scanner (Carl Zeiss AG, Oberkochen, Germany) at 10X (0.45 NA) brightfield magnification to ensure that investigators remained blinded to group identity during image acquisition and analysis. Δ FOSB-expressing cells per region of interest (ROI) were

quantified using atlas-based analysis (42) in FIJI (ImageJ2). Corresponding Bregma levels were assigned using a rat brain atlas (46), and images were converted to 8-bit grayscale. The Warp Image plugin (42) was used to align sections with matching atlas figures via anatomical landmarks. To ensure accuracy, atlas overlays were visually inspected during overlay construction and following particle analysis. Reproducibility was confirmed by duplicating a subset of the overlays and validating automated ROI delineation against manually drawn ROIs in selected regions by two independent experts. Furthermore, Δ FOSB DAB-nickel immunostaining provided sufficient contrast to reliably identify cortical, striatal, hippocampal, amygdalar, and midbrain regions (*e.g.* PAG, LHb, Pir). For regions where boundaries were less distinct, segmentation was guided by surrounding anatomical landmarks. To minimize misclassification, small (sub-)subregions that could not be reliably identified without counterstaining (*e.g.* BNST subnuclei, thalamic/hypothalamic and VTA subregions), were grouped together.

Thresholding, automatic ROI drawing and quantification of Δ FOSB-immunoreactive nuclei was performed with the Batch Counter plugin (42), with embedding of the Robust Automatic Threshold Selection (RATS) plugin (noise = 24, lambda = 3) and the Analyze Particle function (size = 20 - 250, circularity = 0.40 - 1.00). A stringent intensity threshold was applied to ensure that only strongly labeled Δ FOSB-positive nuclei were detected. Missing or damaged ROIs were excluded. Counts were normalized to ROI area and mean of the respective sedentary control group. Fig. 1C shows an overview of the included ROIs, whereas Supplementary Tables 1-4 illustrate all details, including full name, Bregma range and number of slices included per experimental group. Brain regions listed in Supplementary Tables 1 and 2 were included in the main network analysis. In contrast, subregions listed in Supplementary Tables 3 and 4 are part of larger brain structures already represented in the main network analysis and were therefore not separately included, as their activity is expected to be highly correlated with the activity of their respective parent region.

Co-activation network generation and permutation analyses

Pearson correlation coefficients were calculated between brain regions using the `cor()` function in R (version 4.4.1), resulting in group-specific correlation matrices. All correlations were visualized

as heatmaps using the `corrplot()` function (R version 0.95), as previously done (47). Thresholded versions ($\alpha = 0.05, 0.01, \text{ and } 0.0001$) were calculated to assess likelihood of false positives. From these matrices, co-activation networks were constructed using the `igraph` package (R version 2.1.4), representing brain regions as nodes and significant correlations ($\alpha = 0.005$) as undirected edges. Edge thickness (weight) reflects the Pearson correlation coefficient. Networks were laid out using the Fruchterman-Reingold algorithm (`layout_with_fr()`) from the `igraph` package (version 2.1.4), which places nodes with higher connectivity more centrally. To characterize the co-activation networks, we first analyzed global network properties, following established methods (48). Specifically we calculated (using the `igraph` package):

- *Network density*, indicating the proportion of actual edges relative to all possible edges (49), using the `edge_density()` function.
- *Weighted characteristic path length*, representing the average shortest weighted path between all pairs of nodes, reflecting network's efficiency in information transfer, calculated using the `mean_distance()` function.
- *Weighted transivity*, a variant of the clustering coefficient, in which the coefficient is normalized collectively instead of for each node, to lower the influence of nodes with a low degree (50,51), calculated with the `transivity()` function.
- To evaluate small-world characteristics, we compared our networks to 1000 randomly resampled Erdős-Rényi graphs with matched node count and edge density (52). A small-worldness coefficient greater than one indicated small-world-like topology, characterized by higher clustering (*transivity*) and short average path lengths.

We also examined local network properties:

- *Node degree*, the number of edges connected to each node (49), using the `degree()` function.
- *Weighted betweenness centrality*, reflecting how often a node is on the shortest path between other nodes, calculated using the `centrality_betweenness()` function.

Finally, we performed permutation analyses to test for differences in correlations between groups. The `correlation_diff_permutation()` function (53) was used to calculate individual correlation differences $\Delta r (r_{\text{RUN}} - r_{\text{SED}})$, with 1000 bootstrap resamples and considered significant

at $\alpha = 0.005$. All the differences in correlations between groups were visualized as heatmaps using the `heatmap()` function (Supplementary Fig. 9). Overall differences between the SED and RUN correlation matrices were assessed using the `mantel.test()` function with 999 permutations.

Statistical analysis

VWR, metabolic and physiological analyses: comparisons between two groups were performed using two-tailed unpaired Student's t-tests or Mann-Whitney U tests when parametric assumptions were violated. Experiments involving multiple conditions were analyzed via two-way analysis of variance (ANOVA), with repeated measures where applicable, followed, when appropriate by Šidák *post hoc* tests to adjust for multiple comparisons. Correlations were assessed using simple linear regression. $P < 0.05$ was considered statistically significant and $P < 0.10$ was considered a trend towards an effect. No statistical methods were used to estimate sample size.

Regional Δ FOSB expression analyses: two-group comparisons and correlation analyses followed the same approach but included False Discovery Rate (FDR) correction for multiple testing. Given the exploratory nature of the study, both uncorrected and FDR-corrected P values are reported. $P < 0.05$ was considered statistically significant, while $P < 0.10$ was considered a trend towards an effect.

Co-activation network analyses: interregional Δ FOSB expression correlations were computed and visualized in unfiltered heatmaps. Co-activation networks were constructed by filtering these matrices at $P < 0.005$ to reduce spurious correlations. Global and local network metrics were derived from the filtered networks and are presented in bar graphs. Permutation testing of individual correlation differences between experimental groups was performed using bootstrapping ($n = 1000$), with unweighted and significant results ($P < 0.005$) visualized in heatmaps and volcano plots (with additional threshold for correlation differences of >1). Overall differences between experimental groups were assessed using a Mantel test with 999 permutations, with $P < 0.05$ considered statistically significant.

Software: all network analyses and statistical computations were performed in R (version 4.4.1). Behavioral, physiological, and regional Δ FOSB expression data visualizations were generated in

GraphPad Prism (version 10.2.3). See figure legends, Supplementary Tables 1-4 for full statistical details.

ARTICLE IN PRESS

Results (1814 words)**Long-term VWR behavior**

To assess how habitual VWR modulated brain Δ FOSB and Δ FOSB co-activation networks, young-adult male and female Wistar rats were housed without (sedentary) or with free access to a running wheel for 28d (Fig. 1A). Males and females showed a steady increase in daily running distances during the first two weeks of running, followed by stabilization around 2 km/day for males and 6 km/day for females (Fig. 2A,C). Males and females ran a total of 43.2 ± 18.7 km and 145.2 ± 53.8 km, respectively, on average during the 28-day running period (Fig. 2B,D). Rats are nocturnal and accordingly, running was mainly performed during the dark phase (Supplementary Fig. 1A-J).

A two-bottle SPT prior to running suggested that affinity for sucrose did not predict subsequent running behavior in either males or females (Supplementary Fig. 2A-H). Together, males and females showed habitual VWR and females engaged in more running than males, consistent with prior reports (33,54).

Physiological and metabolic impact of long-term VWR

Males and females, whether sedentary or running, gained body weight throughout the experiment, but running generally blunted weight gain compared to sedentary controls (Supplementary Fig. 3A-D). Running significantly lowered body weight compared to sedentary counterparts during week 2 and onwards in males (Supplementary Fig. 3A), whereas running significantly lowered body weight during week 1, but not in the other experimental weeks, in females (Supplementary Fig. 3C).

Running significantly lowered caloric intake during week 1 compared to sedentary controls in both males and females (Supplementary Fig. 3E,G). However, running did not affect consumption of calories during weeks 2-4 compared to sedentary controls in males, whereas running significantly increased caloric intake compared to sedentary controls during week 3 and 4 in females (Supplementary Fig. 3E,G). Overall, running significantly lowered total caloric intake in males, whereas running did not affect total caloric intake in females (Supplementary

Fig. 3F,H). Running did not affect water intake in males or females throughout the experiment (Supplementary Fig. 3I-L).

Running decreased terminal gWAT weight compared to sedentary controls in males and females (Supplementary Fig. 4A,C), but final gWAT weight did not correlate with total running distance in either sex (Supplementary Fig. 4B,D). Running increased final adrenal weight, when normalized for body weight, in both males and females (Supplementary Fig. 4E,G).

Furthermore, final adrenal weight correlated positively with total running distance in males, but not in females (Supplementary Fig. 4F,H).

Determination of estrous stage at death revealed that most females were in proestrus (SED, $n = 7$; RUN, $n = 6$), with smaller numbers in estrus (SED, $n = 3$; RUN: $n = 2$), metestrus (SED, $n = 1$; RUN, $n = 1$), or diestrus (SED, $n = 1$; RUN, $n = 3$). This distribution along the estrous cycle made statistical comparison of fluctuations in Δ FOSB in the 44 brain regions under analysis not possible (41,55). Taken together, running improved metabolic health and modulated adrenal physiology in both sexes.

Long-term VWR modulates brain Δ FOSB in males and females

Next, we used an atlas-based analysis approach (42) to determine how 28 days of VWR affected Δ FOSB-positive cell numbers in 44 brain regions linked to stress-, cognition- and reward-related behavior in males and females compared to sedentary controls (Fig. 1B,C; see Supplementary Tables 1-4 for a full overview of all included ROIs, Bregma ranges, number of slices included per group, percentage of change in runners and statistics).

In males, running increased Δ FOSB-positive cell numbers in infralimbic cortex (IL), cingulate cortex 1 (Cg1), nucleus accumbens shell (AcbSh), dorsomedial (DMS) and dorsolateral striatum (DLS), dorsal part of the lateral septum (LSD), dorsal (dGrDG) and ventral (vGrDG) part of the granule cell layer of the dentate gyrus, ventral molecular layer of the dentate gyrus (vMoDG), ventral part of the cornu ammonis 1 (vCA1) and 3 (vCA3), posterior part of the basolateral amygdala (BLAp), and paraventricular hypothalamic nucleus (PVN) compared to sedentary controls (all $P < 0.05$; Fig. 3A,B; Supplementary Tables 1,3). In addition, running showed a trend towards increased Δ FOSB-positive cell numbers in the prelimbic cortex (PrL), cingulate cortex 2

(Cg2), ventral polymorph layer of the dentate gyrus (vPoDG), basomedial amygdala (BMA), BLA, lateral hypothalamus (LHA) and piriform cortex (Pir) compared to sedentary controls ($P < 0.10$; Fig. 3A,B; Supplementary Table 1). Running did not significantly decrease Δ FOSB-positive cell numbers in any of the examined brain regions (Fig. 3A,B; Supplementary Tables 1,3). A positive and negative correlation between total running distance and Δ FOSB-positive cell numbers was observed in the vCA1 and PVN, respectively (Supplementary Fig. 5A,B). None of the significant increases in Δ FOSB-positive cell numbers in the above-mentioned ROIs, nor any of the significant correlations, survived FDR correction for multiple comparisons (Supplementary Tables 1,3; Supplementary Fig. 5A,B).

In females, running increased Δ FOSB-positive cell numbers in MO, VO, IL, PrL, Cg1, Cg2, dCA1, vPoDG, vCA1, vCA2, vCA3, periaqueductal gray (PAG), and ventral tegmental area (VTA), compared to sedentary controls (all $P < 0.05$; Fig. 4A,B; Supplementary Table 2). In addition, running showed a trend towards increased Δ FOSB-positive cell numbers in M2, AcbSh, LSI, and dCA2, and a trend towards decreased Δ FOSB-positive cell numbers in the arcuate nucleus of the hypothalamus compared to sedentary controls ($P < 0.10$; Fig. 4A,B; Supplementary Table 2). After application of FDR correction for multiple comparisons, running significantly increased Δ FOSB-positive cell numbers in the VO, PrL, Cg2, dCA1, vPoDG, vCA1, vCA2, vCA3 compared to sedentary controls (all $P < 0.05$; Supplementary Table 2). Finally, a positive correlation between total running distance and Δ FOSB-positive cell numbers was observed for the vMoDG and vPoDG, whereas negative correlations trended to be significant for the Cg1, M1, M2 and bed nucleus of the stria terminalis (BNST) of female runners (Supplementary Fig. 6A-G). These significant correlations did not survive FDR correction for multiple comparisons. Together, long-term VWR modulated Δ FOSB in several brain regions involved in stress-, cognition- and reward-related behavior in both sexes.

Long-term VWR modulates brain Δ FOSB co-activation networks in males

To start to investigate how VWR modulates Δ FOSB in brain circuits involved in stress-, cognition- and reward-related behavior on a network level, we assessed Δ FOSB co-activation patterns based on cross-correlated regional Δ FOSB expression across selected brain regions in

male and female sedentary controls and runners. We characterized these networks using global (*i.e.* density and small-world properties) and local (*i.e.* the degree and betweenness centrality per node) network metrics. Additionally, permutation testing was conducted to identify edges that significantly differed between groups.

In sedentary males, the co-activation heatmap and network representations revealed a densely interconnected network, with the hippocampus playing a central role, surrounded by amygdala and cortical regions (Fig. 5A,B). In contrast, male runners displayed a reorganization that was characterized by increased cortical centrality and overall reduced connectivity (Fig. 5B, Supplementary Fig. 9A). These network features remained robust across multiple threshold ($\alpha = 0.05$, $\alpha = 0.01$, and $\alpha = 0.0001$; Supplementary Figs. 7A,B), indicating robust effects of VWR on network organization in males.

Global network analysis confirmed these observations, revealing reduced density in male runners compared to sedentary controls (SED: $k_{DEN} = 0.222$; RUN $k_{DEN} = 0.163$; Fig. 5C). Additionally, small world-like network properties analyses revealed that the networks of both sedentary males and runners exhibited small-world structure with stronger small-world characteristics in runners ($\sigma = 2.51$ and $\sigma = 3.52$, respectively; Fig. 5D), suggesting greater efficiency in their co-activation networks while maintaining local clustering.

Analysis of local metrics further showed a characteristic long-tailed distribution of node degree and betweenness centrality in both groups, indicating that a small subset of nodes exerted a disproportionate influence over the network (Fig. 5E-H). In sedentary males, node degree was highest for hippocampal (dCA1, dPoDG, vCA3, vPoDG) and amygdala (BLA) regions (Fig. 5E). In male runners, degree shifted towards cortical areas (Cg1, Cg2, PrL), with additional high-degree nodes in the amygdala (BMA) and striatum (AcbSh; Fig. 5F). Betweenness centrality was similarly hippocampus- and amygdala-centric (dMoDG, dCA1, LA) in sedentary males, but in runners, the nucleus accumbens (AcbSh) emerged as the most central node, followed by cortical (Cg1), piriform, amygdalar (lateral amygdala; LA) and hippocampal (vPoDG) regions (Fig. 5G,H).

Permutation analysis identified several edges with significantly altered correlations between sedentary and running males (Fig. 5I,J; Supplementary Fig. 9A). For example,

connections between the VTA and both dGrDG and vGrDG, as well as between BLA and dPoDG, were positively correlated in sedentary males but became negatively correlated in runners. Conversely, BNST-PrL and BNST-AcbCo connections switched from negative to positive correlations after VWR. Consistent with these edge-level changes, a Mantel test revealed a significant overall difference between the co-activation heatmaps of male runners and sedentary controls (Supplementary Fig. 9A).

Together, these results suggest that long-term VWR in males enhanced network efficiency, as indicated by increased small world-like network properties, reorganized network topology, and shifts central connectivity from the hippocampal towards cortical and striatal hubs.

Long-term VWR alters Δ FOSB co-activation network efficiency and topology in females

In sedentary females, co-activation maps showed a densely connected network centered around striatal, hippocampal, and orbitofrontal cortical regions (Fig. 6A,B). VWR led to a marked reduction in overall connectivity, accompanied by enhanced intra-cortical connectivity (Fig. 6A,B; Supplementary Fig. 9B). Main network features were retained at $\alpha = 0.05$ and $\alpha = 0.01$, but not at the more conservative $\alpha = 0.0001$ level (Supplementary Fig. 8A,B), indicating a slightly greater sensitivity to statistical thresholding in females.

Global network metrics supported these observations, revealing reduced density in female runners compared to sedentary controls (SED: $k_{DEN} = 0.213$; RUN: $k_{DEN} = 0.057$; Fig. 6C). Additionally, small-worldness was high in both groups, with stronger small-world characteristics in female runners (SED: $\sigma = 4.37$; RUN: $\sigma = 8.62$; Fig. 6D), suggesting greater global efficiency while maintaining local clustering despite sparser connectivity.

Local metrics revealed long-tailed distributions for node degree and betweenness centrality (Fig. 6E-H). In sedentary females, high-degree nodes were found in the striatum (caudate putamen (CPu), AcbSh), hippocampus (dCA1, vCA2), amygdala (LA) and cortex (VO, LO; Fig. 6E). VWR shifted node degree towards cortical regions (PrL, VO, IL, LO; Fig. 6F). Betweenness centrality analyses mirrored these findings: in sedentary females, central nodes included hippocampal (vCA2, dCA1, dCA3), striatal (CPu), cortical (LO, VO) and amygdalar (LA) areas (Fig.

6G). In runners, cortical (PrL, IL, VO) and striatal (AcbCo) regions displayed greater betweenness centrality (Fig. 6H).

Permutation analysis identified edges that significantly changed following VWR (Fig. 6I,J; Supplementary Fig. 9B). Notably, connections between the lateral habenula (LHb) and LHA, BNST and vMoDG, and vCA2 and AcbSh, which were positively correlated in sedentary females, became negatively correlated in runners (Fig. 6I,J). A Mantel test revealed a significant overall difference between the co-activation heatmaps of female runners and sedentary controls (Supplementary Fig. 9B). These findings indicate that VWR in females reorganizes co-activation networks by reducing global connectivity, enhancing efficiency, and shifting centrality from hippocampal and striatal regions towards cortical hubs.

Together, long-term VWR reorganizes brain-wide Δ FOSB co-activation networks in males and females. This reorganization is characterized by reduced network density, increased efficiency, and a shift from hippocampal and amygdala region centrality towards cortical region centrality. As such, this suggests that in contrast to the more diffuse and hippocampal-centric architecture observed in sedentary controls, habitual VWR fosters more efficient and cortically integrated co-activation patterns in the brain.

DISCUSSION (1593 words)

Here, we confirm prior studies that VWR improves metabolic health in rats and that females run greater distances than males. We report the novel findings that long-term VWR caused significant chronic neural activation, but not repression, in a subset of 44 brain regions involved in stress-, cognition- and reward-related behavior in both males and females, many of which have not been studied before in the context of VWR. Subsequent analysis of Δ FOSB co-activation networks revealed that VWR decreases network density, while increasing global efficiency and reorganizing network topology in both sexes.

VWR effects on regional brain Δ FOSB changes

Our exploratory study assessed VWR-induced modulation of brain-wide activation using mapping of Δ FOSB in a large set of brain regions involved in stress-, cognition- and reward-related behavior. Consequently, several significant differences, as well as correlation effects, did not survive the FDR correction for multiple comparisons and as a cautionary note, our differences in individual brain regions thus await confirmation in additional studies. However, consistent with prior studies in male rats (34,35,37,38), we observed VWR induction of Δ FOSB in AcbSh in males and observed smaller effects in females, with a relatively lower induction in AcbCo. Previous studies on VWR induction of NAc Δ FOSB did not specify when brains were collected (38), had collected brains quickly after running in the dark phase (37), or had collected brains during the peak of dark phase running (34,35). These designs did not apply a locked wheel at the end of the experiment which implies that the immunoreactivity they reported could reflect both FOSB *and* Δ FOSB. In contrast, we collected brains after a ~24h wheel blockade, ensuring that immunoreactivity primarily reflects VWR-induction of only Δ FOSB, which potentially explains the smaller effect sizes observed in this study.

We also observed (significant or trending to be significant) induction of Δ FOSB in brain regions that have previously not been reported in males following VWR, including cortical regions (IL, PrL, Cg1, Cg2), lateral septum (LSD), amygdalar (BLAp) and hypothalamic regions (PVN, LHA). Several of these effects were also observed in females (*e.g.* IL, PrL, Cg1, Cg2). Furthermore, males, but not females, showed (significant or trending to be significant) VWR

induction of Δ FOSB in LSD, dGrDG, vGrDG, BMA, BLA, PVN, and LHA, whereas females, but not males, showed (significant or trending to be significant) VWR induction of Δ FOSB in MO, VO, M2, LSI, dCA1, dCA2, vCA2, PAG and VTA. These findings suggest biological meaningful sex differences and future follow-up studies should disentangle the functional relevance of these sex-specific activation signatures.

Our findings extend upon the current literature in males, as well as on VWR effects in females, as to date, the latter had only been studied in prairie voles (40).

VWR activated many brain regions involved in stress-, cognition- and reward-related behavior, but here we highlight several regions. First, we observed VWR induction of Δ FOSB in male PVN, which negatively correlated with total running distance. Because the PVN is important for stress regulation and depression (56,57), and Δ FOSB overexpression has been linked to reduced neuronal excitability in dHPC and vHPC (12,13), these data suggest that VWR may blunt excitability in a subset of PVN neurons, consistent with previous reports of a dampened PVN response to stressors following VWR (58). Second, we observed VWR induction of Δ FOSB in the NAc (mostly in males) and vHPC (in males and females), with positive correlations between Δ FOSB and total running distance observed in several vHPC subregions. In agreement, studies in male mice had demonstrated that stress- or VWR-induction of Δ FOSB in the NAc (15,29,36), or stress induction of Δ FOSB in NAc-projecting vHPC, but not dHPC neurons, is necessary for resilience to stress (13). Third, we observed VWR induction of Δ FOSB in several cortical regions, including IL and PrL. Stress induction of Δ FOSB in the PrL, but not IL, *decreased* resilience for stress in mice (59). Finally, viral-mediated blockade or overexpression of Δ FOSB in mouse dHPC impaired learning and/or memory via alterations in neuronal excitability (12,17), whereas viral-mediated blockade or overexpression of Δ FOSB in mouse vHPC altered neuronal excitability and stress susceptibility (13). Additional studies which *e.g.* specifically manipulate Δ FOSB in the above-mentioned or newly-identified brain regions and/or study the functional properties of their neurons, will be required to clarify their interdependence and/or unique roles in the VWR-mediated changes in learning, cognition, and stress resilience.

Taken together, our findings confirm observations from prior studies in male rats and reveal several novel brain regions where Δ FOSB is altered by VWR in male and female rats, highlighting a broader network of chronic neural activation than previously recognized.

VWR effects on global brain Δ FOSB co-activation changes

Next, to better understand how the regional Δ FOSB changes relate to more global changes, we studied Δ FOSB co-activation networks. Long-term VWR decreased network density and increased network efficiency, in both sexes, suggesting more selective and efficient connectivity. Elevated Δ FOSB levels, either viral-mediated or stimulus-driven, were further shown before to be linked to reduced hippocampal neuronal excitability (12,13), repression of cFOS in the DG, but not CA1, and striatum (11,60) and decreased glutamatergic signaling (16). Thus, VWR-mediated accumulation of Δ FOSB may reduce excitability in particular brain regions, or network nodes, which can lead to more efficient network connectivity. Our findings that VWR increases global efficiency may similarly reflect a shift towards more robust and efficient network interactions. This interpretation aligns with human studies, where exercise training also strengthened functional network connections (61,62). Thus, Δ FOSB accumulation might dampen neuronal reactivation in regions involved in stress and mood regulation, reducing overall network density, while potentially promoting stronger, functionally relevant connections.

VWR further shifted centrality of the hippocampus and amygdala nodes to cortical regions, suggesting an altered top-down control. In human studies, exercise training modulated resting-state functional connectivity in cognitive networks (63) and enhanced coherence within the default mode network (64–66) and executive control network (67). In contrast, overall cortical hypoactivity is associated with poorer top-down regulation of emotions in depression (68–70) and post-traumatic stress disorder (71). These observations suggest that VWR-induced changes in network topology, particularly towards cortical hubs, may promote a protective ‘rebalancing’ of downstream emotional and cognitive processing systems to protect against stress-related disorders. Animal studies that manipulate Δ FOSB in specific brain regions before assessment of network topology will be required to test these hypotheses.

To the best of our knowledge, by studying the construction of co-activation networks, we introduce a novel network perspective on how VWR impacts brain function. Due to the high stability of Δ FOSB (16), we capture enduring network changes, making it well-suited to examine how brain circuits are activated by repetitive events or behaviors, like VWR. This approach is, however, also limited in that it does not capture acute and recent, or more transient responses. Different experimental designs, or the integration of Δ FOSB and cFOS co-activation networks, e.g. after an acute stressor, could address other temporal levels of brain activation.

Our networks are further based on interregional correlations in Δ FOSB expression, reflecting co-activational rather than structural interactions. Despite these limitations, VWR reorganized network topology, reducing density, while enhancing efficiency and shifting centrality towards cortical regions. Thus, Δ FOSB co-activation networks provide a valuable perspective on how VWR reshapes global chronic neuronal activation.

Potential upstream mechanisms underlying VWR-induction of Δ FOSB

It is so far unclear which specific signaling cascades mediate VWR induction of Δ FOSB. The self-reinforcing and rewarding nature of VWR (31) suggests involvement of dopamine. Indeed, Δ FOSB is well-known for its role in NAc medium spiny neurons, particularly in response to dopamine signaling (16). Furthermore, dopamine can synergize with TGF β receptor ALK4 to enhance Δ FOSB production via the RNA-binding proteins PCBP1 and SMAD3 in NAc MSNs (72). Another modulator might be estrogen, as we have recently demonstrated that estrogen modulated Δ FOSB in rat suprachiasmatic nucleus (41). Similarly, fluctuating estrogen levels across the estrous cycle regulate NAc Δ FOSB-related chromatin changes that influence cocaine responses (55). While our attempt to synchronize the estrous cycle at the start of the experiment has likely reduced estrogen-driven variation, differences in estrous phase at the end of the experiment may potentially have influenced Δ FOSB expression. As the number of animals per phase did not differ much between the groups, it is unlikely the estrous cycle has contributed significantly to our current Δ FOSB results, but we cannot fully exclude this and this remains a limitation of our study.

Beyond potential effects on Δ FOSB, estrogen may also influence sucrose affinity. We observed that sucrose preference prior to running did not predict subsequent VWR behavior, short- or long-term, in either males or females. In females, however, the three-day sucrose test may not have fully captured estrous cycle-related variation (which usually spans four days) influences on hedonic behaviors, such as sucrose water consumption. Therefore, the absence of a correlation between sucrose affinity prior to running and subsequent running behavior cannot be fully excluded by the current study. Studies which manipulate dopamine, TGF β and/or estrogen signaling in specific neuronal populations and brain regions during VWR will be required to clarify the role of these signaling molecules in VWR-mediated changes in Δ FOSB.

Because Δ FOSB regulates expression of many genes (73), our findings suggest widespread neuronal adaptations following VWR. Previous VWR research in mice has largely focused on NAc and HPC, but our findings highlight that many additional brain regions might play a role in behavioral processes affected by VWR, including VWR-induction of stress resilience. Because Δ FOSB manipulation in the NAc reshapes whole brain functional connectivity (74), such manipulations should focus on these 'hub' regions and also study subsequent general changes in network topology.

Conclusion

Habitual VWR induced brain-wide Δ FOSB accumulation in several brain regions involved in stress-, cognition- and reward-related behavior in male and female rats and reshaped Δ FOSB co-activation networks. Our VWR Δ FOSB brain atlas provides a starting point for functional studies in male and female rats to provide more mechanistic understanding as to how VWR-mediated Δ FOSB accumulation promotes neuroplasticity and alters stress-, cognition- and reward-related behavior.

Author Contributions

Conceptualization: M.H.H., A.H.V., A.K., P.J.L., A.S., S.E.I.F., J.D.M.; Methodology: M.H.H., A.H.V., T.P.H., G.M., J.D.M.; Software: A.H.V.; Validation: M.H.H., T.P.H., J.D.M.; Formal analysis: M.H.H.; Investigation: M.H.H., T.P.H., L.E., W.I.G.R.R., K.L., U.A.U., G.M., J.D.M.; Resources: A.K., P.J.L., S.E.I.F., J.D.M.; Data curation: M.H.H., A.H.V.; Writing – original draft: M.H.H.; Writing – review & editing: M.H.H., A.H.V., A.K., P.J.L., A.S., S.E.I.F., J.D.M.; Visualization: M.H.H.; Supervision: P.J.L., A.S., S.E.I.F., J.D.M.; Project administration: M.H.H., J.D.M.; Funding acquisition: S.E.I.F., J.D.M., P.J.L., A.K., A.S.

Acknowledgements

We thank all members of the Fit Brain Lab (University of Amsterdam) and Brain Plasticity group (University of Amsterdam) for their useful discussions. This work was supported by Amsterdam Neuroscience (JDM), Centre for Urban Mental Health (AHV, PJJ, AS, SEIF and JDM), ZonMw MODEM (PJJ), NWO-icNS (PJJ), Alzheimer Nederland (PJJ), the BioClock Consortium, part of the NWA-ORC program of the Dutch Research Council (NOW; project number 1292.19.077) (AK) and the Dutch Research Council (NWO) Vici talent program (SEIF). We thank internship students Julia van den Broek, Nikita Cijssouw, Sophie Didden, Meike Doorenbos, Dorte Heideman, Aleesha Hol, Maaïke Kesting, Amber Koert, Niels Reijner and Rick Wenning for their contributions during various stages of the project. We thank prof. dr. Roger Adan (UMC Utrecht) for use of the rat running wheel system and we thank the NIN microscopy support team Joop van Heerikhuizen, Joris Coppens and Roeland Lokhorst for their help while operating the slide scanner.

Conflict of interest

The authors declare no competing financial interests.

Supplementary information

Supplementary information is available online at the *Translational Psychiatry* website.

Data availability

Access to the data and computational tools used in this study can be obtained from the corresponding author upon reasonable request.

ARTICLE IN PRESS

REFERENCES

1. Manning CE, Williams ES, Robison AJ. Reward Network Immediate Early Gene Expression in Mood Disorders. *Front Behav Neurosci*. 2017 Apr 28;11:77.
2. Nestler EJ. Δ FosB: a transcriptional regulator of stress and antidepressant responses. *Eur J Pharmacol*. 2015 Apr 15;753:66–72.
3. Robison AJ, Nestler EJ. Transcriptional and epigenetic mechanisms of addiction. *Nat Rev Neurosci*. 2011 Nov;12(11):623–37.
4. Berton O, Guigoni C, Li Q, Bioulac BH, Aubert I, Gross CE, et al. Striatal Overexpression of Δ JunD Resets L-DOPA-Induced Dyskinesia in a Primate Model of Parkinson Disease. *Biol Psychiatry*. 2009 Sept;66(6):554–61.
5. Beck G, Singh A, Zhang J, Potts LF, Woo JM, Park ES, et al. Role of striatal Δ FosB in L-Dopa-induced dyskinesias of parkinsonian nonhuman primates. *Proc Natl Acad Sci*. 2019 Sept 10;116(37):18664–72.
6. Corbett BF, You JC, Zhang X, Pyfer MS, Tosi U, Iacone DM, et al. Δ FosB Regulates Gene Expression and Cognitive Dysfunction in a Mouse Model of Alzheimer's Disease. *Cell Rep*. 2017 July;20(2):344–55.
7. Mandelzys A, Gruda MA, Bravo R, Morgan JI. Absence of a Persistently Elevated 37 kDa Fos-Related Antigen and AP-1-Like DNA-Binding Activity in the Brains of Kainic Acid-Treated *fos* B Null Mice. *J Neurosci*. 1997 July 15;17(14):5407–15.
8. Yutsudo N, Kamada T, Kajitani K, Nomaru H, Katogi A, Ohnishi YH, et al. *fos*B-Null Mice Display Impaired Adult Hippocampal Neurogenesis and Spontaneous Epilepsy with Depressive Behavior. *Neuropsychopharmacology*. 2013 Apr;38(5):895–906.
9. You JC, Muralidharan K, Park JW, Petrof I, Pyfer MS, Corbett BF, et al. Epigenetic suppression of hippocampal calbindin-D28k by Δ FosB drives seizure-related cognitive deficits. *Nat Med*. 2017 Nov;23(11):1377–83.
10. Manning CE, Eagle AL, Kwiatkowski CC, Achargui R, Woodworth H, Potter E, et al. Hippocampal Subgranular Zone FosB Expression Is Critical for Neurogenesis and Learning. *Neuroscience*. 2019 May;406:225–33.
11. Lamothe-Molina PJ, Franzelin A, Beck L, Li D, Auksutat L, Fieblinger T, et al. Δ FosB accumulation in hippocampal granule cells drives cFos pattern separation during spatial learning. *Nat Commun*. 2022 Oct 26;13(1):6376.
12. Eagle AL, Williams ES, Beatty JA, Cox CL, Robison AJ. Δ FosB Decreases Excitability of Dorsal Hippocampal CA1 Neurons. *eneuro*. 2018 July;5(4):ENEURO.0104-18.2018.

13. Eagle AL, Manning CE, Williams ES, Bastle RM, Gajewski PA, Garrison A, et al. Circuit-specific hippocampal Δ FosB underlies resilience to stress-induced social avoidance. *Nat Commun*. 2020 Sept 8;11(1):4484.
14. Eagle AL, Gajewski PA, Robison AJ. Role of hippocampal activity-induced transcription in memory consolidation. *Rev Neurosci*. 2016 Aug 1;27(6):559–73.
15. Vialou V, Robison AJ, LaPlant QC, Covington HE, Dietz DM, Ohnishi YN, et al. Δ FosB in brain reward circuits mediates resilience to stress and antidepressant responses. *Nat Neurosci*. 2010 June;13(6):745–52.
16. Robison AJ, Nestler EJ. Δ FOSB: A Potentially Druggable Master Orchestrator of Activity-Dependent Gene Expression. *ACS Chem Neurosci*. 2022 Feb 2;13(3):296–307.
17. Eagle AL, Gajewski PA, Yang M, Kechner ME, Al Masraf BS, Kennedy PJ, et al. Experience-Dependent Induction of Hippocampal Δ FosB Controls Learning. *J Neurosci*. 2015 Oct 7;35(40):13773–83.
18. Chen J, Kelz MB, Hope BT, Nakabeppu Y, Nestler EJ. Chronic Fos-Related Antigens: Stable Variants of deltaFosB Induced in Brain by Chronic Treatments. *J Neurosci*. 1997;17(13):4933–41.
19. Hiroi N, Marek GJ, Brown JR, Ye H, Saudou F, Vaidya VA, et al. Essential Role of the *fos B* Gene in Molecular, Cellular, and Behavioral Actions of Chronic Electroconvulsive Seizures. *J Neurosci*. 1998 Sept 1;18(17):6952–62.
20. Nestler EJ. Cellular basis of memory for addiction. *Dialogues Clin Neurosci*. 2013 Dec;15(4):431–43.
21. Yin Z, Venkannagari H, Lynch H, Aglyamova G, Bhandari M, Machius M, et al. Self-assembly of the bZIP transcription factor Δ FosB. *Curr Res Struct Biol*. 2020;2:1–13.
22. Andersson M, Westin JE, Cenci MA. Time course of striatal Δ FosB-like immunoreactivity and prodynorphin mRNA levels after discontinuation of chronic dopaminomimetic treatment. *Eur J Neurosci*. 2003 Feb;17(3):661–6.
23. Carle TL, Ohnishi YN, Ohnishi YH, Alibhai IN, Wilkinson MB, Kumar A, et al. Proteasome-dependent and -independent mechanisms for FosB destabilization: identification of FosB degron domains and implications for Δ FosB stability. *Eur J Neurosci*. 2007 May;25(10):3009–19.
24. Cates HM, Thibault M, Pfau M, Heller E, Eagle A, Gajewski P, et al. Threonine 149 Phosphorylation Enhances Δ FosB Transcriptional Activity to Control Psychomotor Responses to Cocaine. *J Neurosci*. 2014 Aug 20;34(34):11461–9.

25. Hope BT, Nye HE, Kelz MB, Self DW, Iadarola MJ, Nakabeppu Y, et al. Induction of a long-lasting AP-1 complex composed of altered Fos-like proteins in brain by chronic cocaine and other chronic treatments. *Neuron*. 1994 Nov;13(5):1235–44.
26. Kreuter JD, Mattson BJ, Wang B, You ZB, Hope BT. Cocaine-induced Fos expression in rat striatum is blocked by chloral hydrate or urethane. *Neuroscience*. 2004 Jan;127(1):233–42.
27. Ulery-Reynolds PG, Castillo MA, Vialou V, Russo SJ, Nestler EJ. Phosphorylation of Δ FosB mediates its stability in vivo. *Neuroscience*. 2009 Jan;158(2):369–72.
28. Nestler EJ, Russo SJ. Neurobiological basis of stress resilience. *Neuron*. 2024 June;112(12):1911–29.
29. Vialou V, Maze I, Renthal W, LaPlant QC, Watts EL, Mouzon E, et al. Serum Response Factor Promotes Resilience to Chronic Social Stress through the Induction of FosB. *J Neurosci*. 2010 Oct;30(43):14585–92.
30. Nestler EJ. Transcriptional mechanisms of addiction: role of Δ FosB. *Philos Trans R Soc B Biol Sci*. 2008 Oct 12;363(1507):3245–55.
31. Greenwood BN, Fleshner M. Voluntary wheel running: a useful rodent model for investigating mechanisms of stress robustness and exercise motivation. *Curr Opin Behav Sci*. 2019 Aug;28:78–84.
32. Mul JD. Voluntary exercise and depression-like behavior in rodents: are we running in the right direction? *J Mol Endocrinol*. 2018 Apr;60(3):R77–95.
33. Tanner MK, Mellert SM, Fallon IP, Baratta MV, Greenwood BN. Multiple Sex- and Circuit-Specific Mechanisms Underlie Exercise-Induced Stress Resistance. In: Cisler JM, Crombie KM, Adams TG, editors. *Exercise and Mental Health* [Internet]. Cham: Springer International Publishing; 2024. p. 37–60. Available from: https://doi.org/10.1007/7854_2024_490
34. Greenwood BN, Foley TE, Le TV, Strong PV, Loughridge AB, Day HEW, et al. Long-term voluntary wheel running is rewarding and produces plasticity in the mesolimbic reward pathway. *Behav Brain Res*. 2011 Mar;217(2):354–62.
35. Herrera JJ, Fedynska S, Ghasem PR, Wieman T, Clark PJ, Gray N, et al. Neurochemical and behavioural indices of exercise reward are independent of exercise controllability. Foxe J, editor. *Eur J Neurosci*. 2016 May;43(9):1190–202.
36. Mul JD, Soto M, Cahill ME, Ryan RE, Takahashi H, So K, et al. Voluntary wheel running promotes resilience to chronic social defeat stress in mice: a role for nucleus accumbens Δ FosB. *Neuropsychopharmacology*. 2018 Aug;43(9):1934–42.

37. Obici S, Magrisso IJ, Ghazarian AS, Shirazian A, Miller JR, Loyd CM, et al. Moderate voluntary exercise attenuates the metabolic syndrome in melanocortin-4 receptor-deficient rats showing central dopaminergic dysregulation. *Mol Metab.* 2015 Oct;4(10):692–705.
38. Werme M, Messer C, Olson L, Gilden L, Brene S. Delta FosB Regulates Wheel Running. *J Neurosci.* 2002;22(18):8133–8.
39. Nishijima T, Kawakami M, Kita I. Long-Term Exercise Is a Potent Trigger for Δ FosB Induction in the Hippocampus along the dorso–ventral Axis. *Fisone G, editor. PLoS ONE.* 2013 Nov 25;8(11):e81245.
40. Watanasriyakul WT, Normann MC, Akinbo OI, Colburn W, Dagner A, Grippo AJ. Protective neuroendocrine effects of environmental enrichment and voluntary exercise against social isolation: evidence for mediation by limbic structures. *Stress.* 2019 Sept 3;22(5):603–18.
41. Shiba A, Hardonk MH, Foppen E, Kool T, La Fleur SE, Lucassen PJ, et al. Voluntary Running and Estrous Cycle Modulate Δ FOSB in the Suprachiasmatic Nucleus of the Wistar Rat. *J Circadian Rhythms.* 2025 May 19;23:7.
42. Bourgeois JR, Kalyanasundaram G, Figueroa C, Srinivasan A, Kopec AM. A semi-automated brain atlas-based analysis pipeline for c-Fos immunohistochemical data. *J Neurosci Methods.* 2021 Jan;348:108982.
43. Hillebrand JJG, Kas MJH, Scheurink AJW, Van Dijk G, Adan RAH. AgRP(83–132) and SHU9119 differently affect activity-based anorexia. *Eur Neuropsychopharmacol.* 2006 Aug;16(6):403–12.
44. Perrotti LI, Hadeishi Y, Ulery PG, Barrot M, Monteggia L, Duman RS, et al. Induction of Δ FosB in Reward-Related Brain Structures after Chronic Stress. *J Neurosci.* 2004 Nov 24;24(47):10594–602.
45. Nestler EJ, Barrot M, Self DW. Δ FosB: A sustained molecular switch for addiction. *Proc Natl Acad Sci.* 2001 Sept;98(20):11042–6.
46. Watson C, Paxinos G. *The Rat Brain in Stereotaxic Coordinates.* 6th ed. Elsevier Inc.; 2007. 456 p.
47. Terstege D, Epp J. Network Neuroscience Untethered: Brain-Wide Immediate Early Gene Expression for the Analysis of Functional Connectivity in Freely Behaving Animals. *Biology.* 2022 Dec 24;12(1):34.
48. Bullmore ET, Bassett DS. *Brain Graphs: Graphical Models of the Human Brain Connectome.* *Annu Rev Clin Psychol.* 2011 Apr 27;7(1):113–40.
49. Rubinov M, Sporns O. Complex network measures of brain connectivity: Uses and interpretations. *NeuroImage.* 2010 Sept;52(3):1059–69.

50. Newman MEJ. The Structure and Function of Complex Networks. *Soc Ind Appl Math*. 2003 Mar;45(2):167–256.
51. Onnela JP, Saramäki J, Kertész J, Kaski K. Intensity and coherence of motifs in weighted complex networks. *Phys Rev, E Stat Nonlinear Soft Matter Phys*. 2005 June;71.
52. Watts DJ, Strogatz SH. Collective dynamics of ‘small-world’ networks. *Nature*. 1998;393:440–2.
53. Jin M, Ogundare SO, Lanio M, Sorid S, Whye AR, Leal Santos S, et al. A SMARTTR workflow for multi-ensemble atlas mapping and brain-wide network analysis [Internet]. *BioRxiv*; 2024 [cited 2025 May 16]. Available from: <https://www.biorxiv.org/content/10.1101/2024.07.12.603299v1>
54. Mathis V, Wegman-Points L, Pope B, Lee CMJ, Mohamed M, Rhodes JS, et al. Estrogen-mediated individual differences in female rat voluntary running behavior. *J Appl Physiol*. 2024 Mar 1;136(3):592–605.
55. Rocks D, Jaric I, Bellia F, Cham H, Greally JM, Suzuki M, et al. Early-life stress and ovarian hormones alter transcriptional regulation in the nucleus accumbens resulting in sex-specific responses to cocaine. *Cell Rep*. 2023 Oct;42(10):113187.
56. Herman JP, Tasker JG. Paraventricular Hypothalamic Mechanisms of Chronic Stress Adaptation. *Front Endocrinol*. 2016 Oct 31;7:137.
57. Swaab DF, Bao AM, Lucassen PJ. The stress system in the human brain in depression and neurodegeneration. *Ageing Res Rev*. 2005 May;4(2):141–94.
58. Campeau S, Nyhuis TJ, Sasse SK, Kryskow EM, Herlihy L, Masini CV, et al. Hypothalamic Pituitary Adrenal Axis Responses to Low-Intensity Stressors are Reduced After Voluntary Wheel Running in Rats. *J Neuroendocrinol*. 2010 Aug;22(8):872–88.
59. Vialou V, Bagot RC, Cahill ME, Ferguson D, Robison AJ, Dietz DM, et al. Prefrontal Cortical Circuit for Depression- and Anxiety-Related Behaviors Mediated by Cholecystokinin: Role of Δ FosB. *J Neurosci*. 2014 Mar 12;34(11):3878–87.
60. Renthal W, Carle TL, Maze I, Covington HE, Truong HT, Alibhai I, et al. Δ FosB Mediates Epigenetic Desensitization of the *c-fos* Gene After Chronic Amphetamine Exposure. *J Neurosci*. 2008 July 16;28(29):7344–9.
61. Moore D, Jung M, Hillman CH, Kang M, Loprinzi PD. Interrelationships between exercise, functional connectivity, and cognition among healthy adults: A systematic review. *Psychophysiology*. 2022 June;59(6):e14014.

62. Won J, Callow DD, Pena GS, Gogniat MA, Kommula Y, Arnold-Nedimala NA, et al. Evidence for exercise-related plasticity in functional and structural neural network connectivity. *Neurosci Biobehav Rev.* 2021 Dec;131:923–40.
63. Bodensohn L, Maurer A, Daamen M, Upadhyay N, Werkhausen J, Lohaus M, et al. Inverted U-shape-like functional connectivity alterations in cognitive resting-state networks depending on exercise intensity: An fMRI study. *Brain Cogn.* 2024 June;177:106156.
64. Chirles TJ, Reiter K, Weiss LR, Alfini AJ, Nielson KA, Smith JC. Exercise Training and Functional Connectivity Changes in Mild Cognitive Impairment and Healthy Elders. *J Alzheimer's Dis.* 2017 Apr 10;57(3):845–56.
65. McGregor KM, Crosson B, Krishnamurthy LC, Krishnamurthy V, Hortman K, Gopinath K, et al. Effects of a 12-Week Aerobic Spin Intervention on Resting State Networks in Previously Sedentary Older Adults. *Front Psychol.* 2018 Nov 27;9:2376.
66. Voss. Plasticity of brain networks in a randomized intervention trial of exercise training in older adults. *Front Aging Neurosci.* 2010;2:32.
67. Prehn K, Lesemann A, Krey G, Witte AV, Köbe T, Grittner U, et al. Using resting-state fMRI to assess the effect of aerobic exercise on functional connectivity of the DLPFC in older overweight adults. *Brain Cogn.* 2019 Apr;131:34–44.
68. Kaiser RH, Andrews-Hanna JR, Wager TD, Pizzagalli DA. Large-Scale Network Dysfunction in Major Depressive Disorder: A Meta-analysis of Resting-State Functional Connectivity. *JAMA Psychiatry.* 2015 June 1;72(6):603.
69. Li B, Friston K, Mody M, Wang H, Lu H, Hu D. A brain network model for depression: From symptom understanding to disease intervention. *CNS Neurosci Ther.* 2018 Nov;24(11):1004–19.
70. Lynch CJ, Elbau IG, Ng T, Ayaz A, Zhu S, Wolk D, et al. Frontostriatal salience network expansion in individuals in depression. *Nature.* 2024 Sept 19;633(8030):624–33.
71. Etkin A, Wager TD. Functional Neuroimaging of Anxiety: A Meta-Analysis of Emotional Processing in PTSD, Social Anxiety Disorder, and Specific Phobia. *Am J Psychiatry.* 2007 Oct;164(10):1476–88.
72. Krapacher FA, Fernández-Suárez D, Andersson A, Carrier-Ruiz A, Ibáñez CF. Convergent dopamine and ALK4 signaling to PCBP1 controls FosB alternative splicing and cocaine behavioral sensitization. *EMBO J.* 2022 Aug;41(15):e110721.
73. McClung CA, Nestler EJ. Regulation of gene expression and cocaine reward by CREB and Δ FosB. *Nat Neurosci.* 2003 Nov;6(11):1208–15.

74. Sourty M, Nasseef MT, Champagnol-Di Liberti C, Mondino M, Noblet V, Parise EM, et al. Manipulating Δ FOSB in D1-Type Medium Spiny Neurons of the Nucleus Accumbens Reshapes Whole-Brain Functional Connectivity. *Biol Psychiatry*. 2024 Feb;95(3):266–74.

ARTICLE IN PRESS

FIGURE LEGENDS

Fig. 1: Experimental timeline and workflow. (a) Experimental timeline of animal studies. All male and female rats were housed without a running wheel (sedentary; SED) during the 7-day acclimatization period and the 7-day baseline measurement period. During the last three days of the baseline period, animals were subjected to a two-bottle sucrose preference test (SPT). During the subsequent 28-day experimental period, SED controls remained housed without a running wheel, whereas runners (RUN) were housed with a running wheel. Body weight, food and water intake were measured weekly. Wheels were blocked for 24h before isolation of brains. (b) Experimental workflow of immunohistochemistry, Δ FOSB quantification, and Δ FOSB co-activation network generation and analysis. (c) Brain regions of interest (ROIs) categorized by parent structures: cortex (green), basal ganglia and septum (purple), hippocampus (yellow), extended amygdala (pink), thalamus and hypothalamus (blue), midbrain (orange), and other (gray), see Supplementary Tables 1-4, for a list of abbreviations.

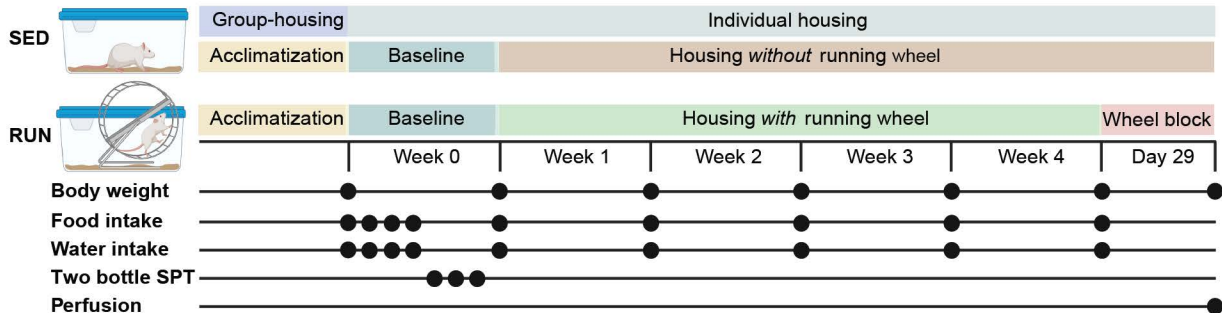
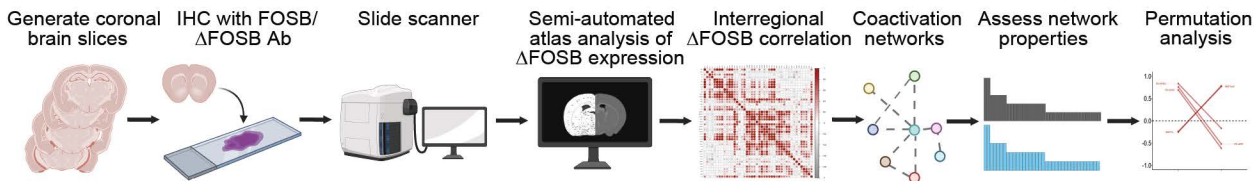
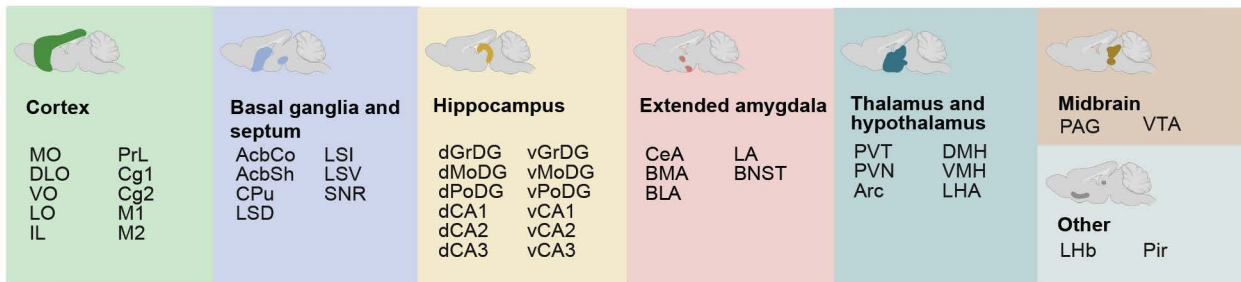
Fig. 2: Running behavior in males and females. (a) Daily and (b) total running distance of males during 28 days of running. (c) Daily and (d) total running distance of females during 28 days of running. Data are presented as the mean \pm S.E.M (a, c) or as box plots indicating the median (line) and mean (+), the interquartile range, and the minimum to maximum values of the data distribution, with dots representing individual rats (b, d). (a-d) $n = 12$ /group.

Fig. 3: Long-term VWR induction of Δ FOSB in males. (a) Fold change in the mean number of Δ FOSB-positive cells per region of interest (ROI) in male sedentary (SED) controls and runners (RUN), normalized to the mean of SED rats; $*P < 0.05$, $+P < 0.10$ before FDR correction; see Supplementary Table 1 for exact statistical values. (b) Representative images of Δ FOSB immunoreactivity in the infralimbic cortex (IL), cingulate cortex 1 (Cg1), nucleus accumbens shell (AcbSh), dorsal part of the lateral septum (LSD), the dorsal part of the granule cell layer of the dentate gyrus (dGrDG), the ventral dentate gyrus (vDG) including the granule cell layer (vGrDG), the molecular layer (vMoDG) and the polymorph layer (vPoDG), the ventral cornu ammonis 1 (vCA1) and 3 (vCA3) and the paraventricular hypothalamus nucleus (PVN). Scale bar = 100 μ m. Data are presented as the mean \pm S.E.M (a). (a) $n = 12$ /group.

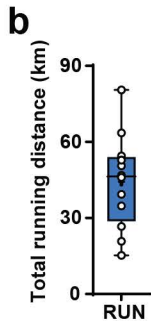
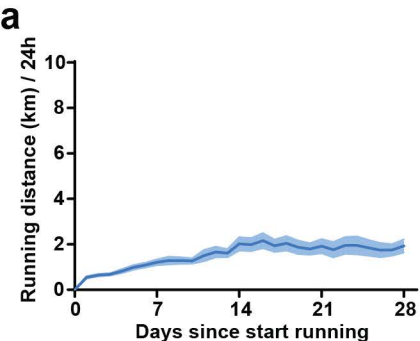
Fig. 4: Long-term VWR induction of Δ FOSB in females. (a) Fold change in the mean number of Δ FOSB-positive cells per region of interest (ROI) in female sedentary (SED) controls and runners (RUN), normalized to the mean of SED rats; $*P < 0.05$, $+P < 0.10$ before FDR correction; see Supplemental Table 2 for exact statistical values. (b) Representative images of Δ FOSB immunoreactivity in the medial (MO) and ventral orbital cortex (VO), the infralimbic (IL) and prelimbic cortex (PrL), cingulate cortex 1 (Cg1) and 2 (Cg2), dorsal cornu ammonis 1 (dCA1), the ventral polymorph layer of the dentate gyrus (vPoDG), the ventral cornu ammonis (vCA) including the vCA1, vCA2 and vCA3, the periaqueductal gray (PAG) and the ventral tegmental area (VTA). Scale bar = 100 μ m. Data are presented as the mean \pm S.E.M (a). (a) $n = 12$ /group.

Fig. 5: Network analysis reveals altered Δ FOSB co-activation following VWR in males. (a) Unweighted regional cross-correlation matrices of Δ FOSB-positive cells per mm^2 between all pairs of neuroanatomical regions of male sedentary controls (SED) and runners (RUN). (b) Δ FOSB co-activation networks constructed after thresholding for the strongest and most significant correlated or anti-correlated connections ($r > 0.7$, $P < 0.005$) in SED and RUN rats. (c) Network density expressed as k_{DEN} , of SED and RUN rats. (d) Small world-like properties expressed as σ of SED and RUN rats. (e, f) Node degree per ROI of (e) SED and (f) RUN rats. (g, h) Betweenness centrality per ROI of (g) SED and (h) RUN rats. (i) Volcano plot of Pearson correlation differences ($r_{RUN} - r_{SED}$) for all individual regional connections against their P -values calculated from a permutation analysis. Points intersecting or within the upper left or right quadrant represent the regional relationships with the greatest change ($|\text{correlation difference}| > 1$) that were most significant. (j) Parallel coordinate plots highlighting individual significantly changed regional correlations between SED and RUN rats. (a-j) $n = 12/\text{group}$. (b-j) $P < 0.005$ was considered significant.

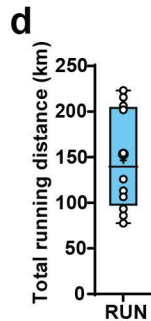
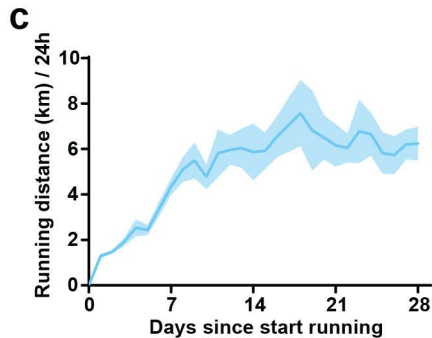
Fig. 6: Network analysis reveals altered Δ FOSB co-activation following VWR in females. (a) Unweighted regional cross-correlation matrices of Δ FOSB-positive cells per mm^2 between all pairs of neuroanatomical regions of female sedentary controls (SED) and runners (RUN). (b) Δ FOSB co-activation networks constructed after thresholding for the strongest and most significant correlated or anti-correlated connections ($r > 0.7$, $P < 0.005$) of SED and RUN rats. (c) Network density expressed as k_{DEN} , of SED and RUN rats. (d) Small world-like properties expressed as σ of SED and RUN rats. (e, f) Node degree per ROI of (e) SED and (f) RUN rats. (g, h) Betweenness centrality per ROI of (g) SED and (h) RUN rats. (i) Volcano plot of Pearson correlation differences ($r_{RUN} - r_{SED}$) for all individual regional connections against their P -values calculated from a permutation analysis. Points intersecting or within the upper left or right quadrant represent the regional relationships with the greatest change ($|\text{correlation difference}| > 1$) that were most significant. (j) Parallel coordinate plots highlighting individual significantly changed regional correlations between SED and RUN rats. (a-j) $n = 12/\text{group}$. (b-j) $P < 0.005$ was considered significant.

a**b****c**

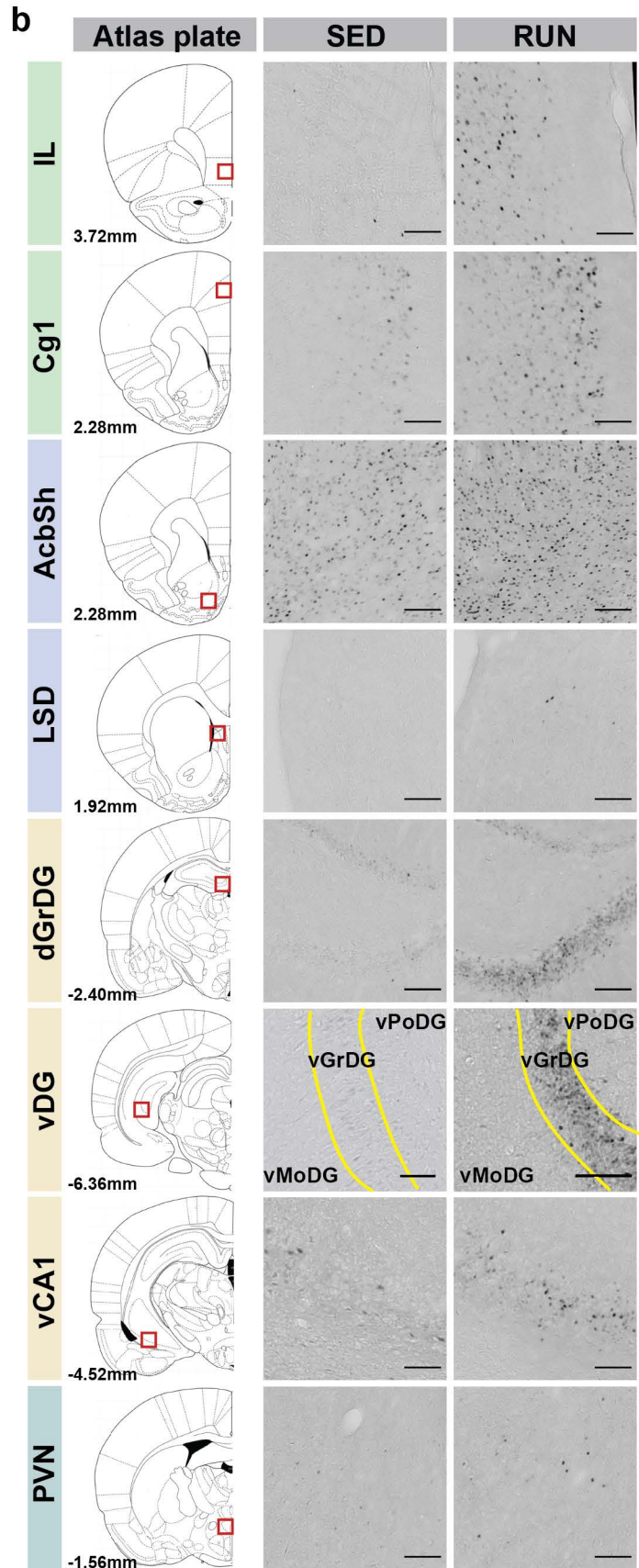
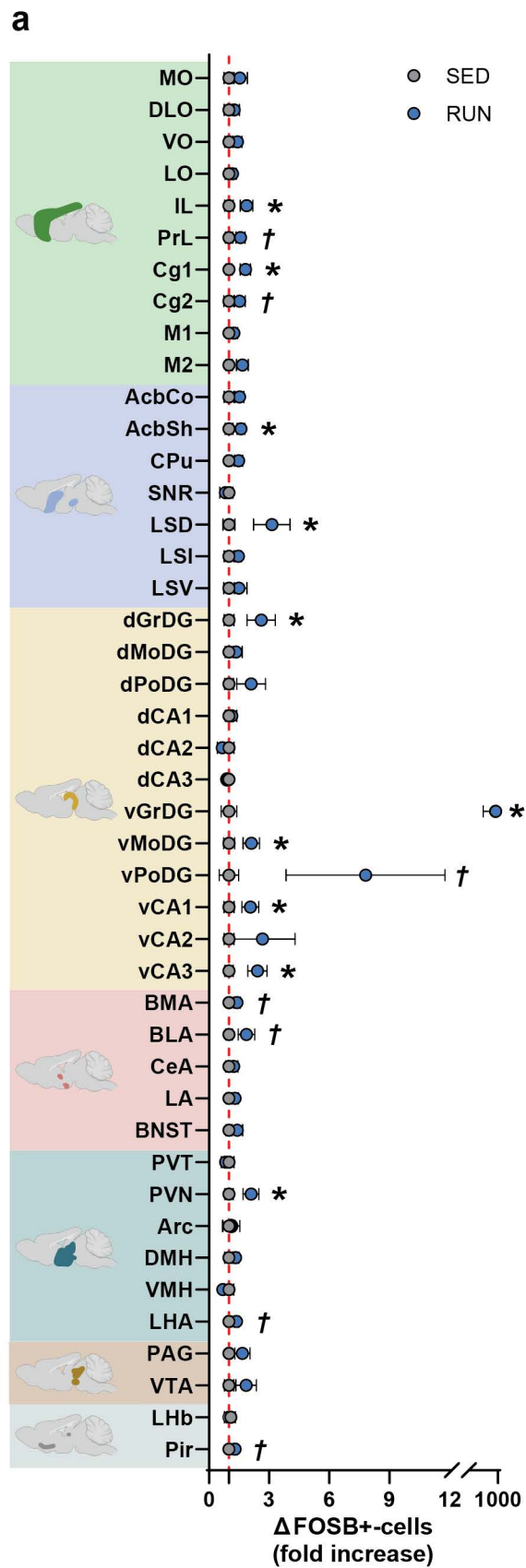
Males



Females

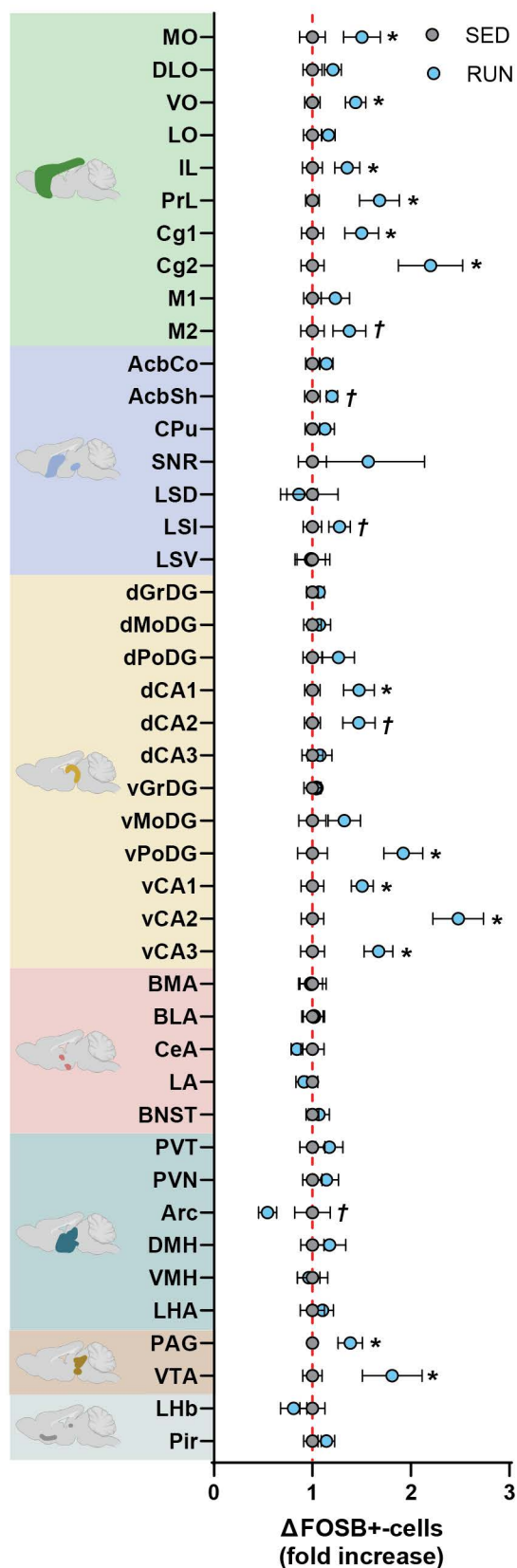


Males

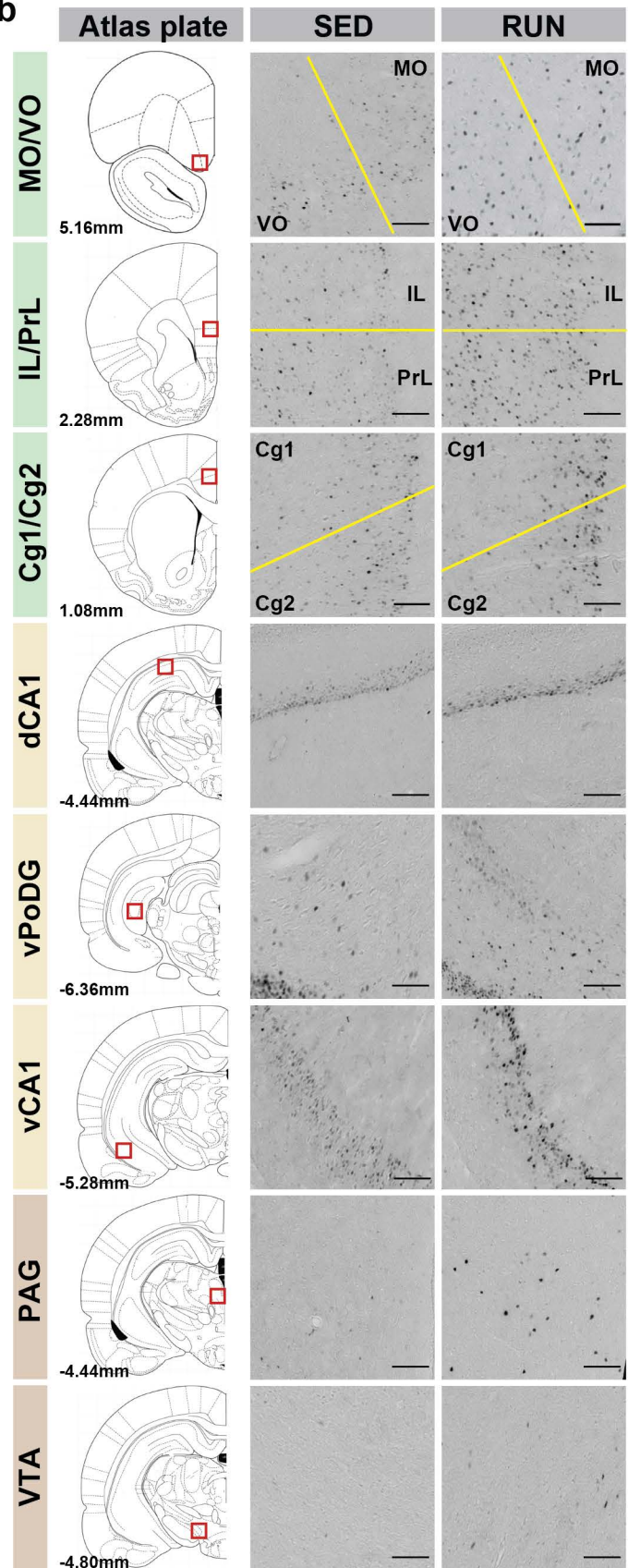


Females

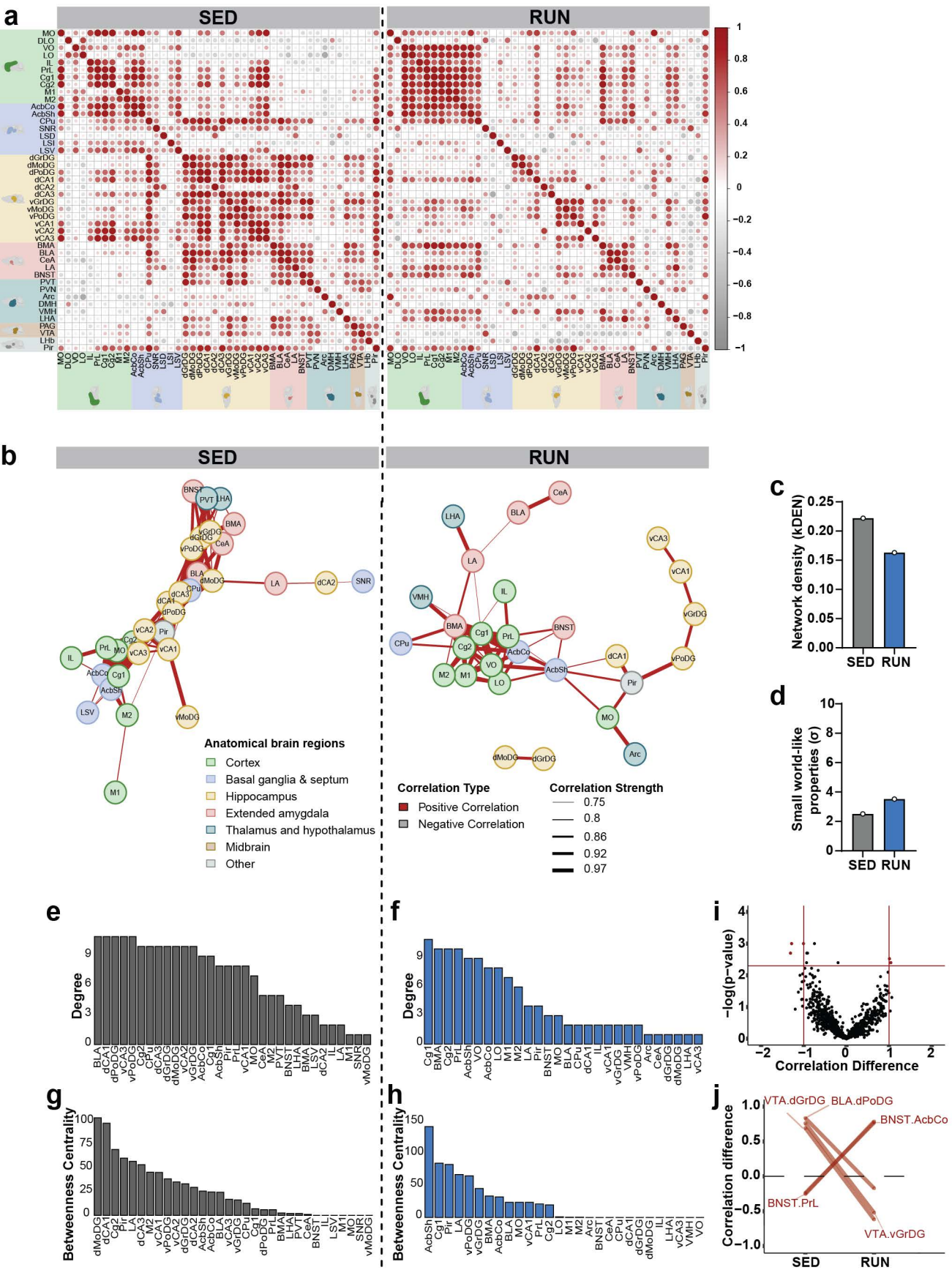
a



b



Males



Females

